

Laterally strained turbulent boundary layers near a plane of symmetry

By LUCIO POMPEO†, MARCO S. G. BETTELINI‡
AND HANS THOMANN

Institut für Fluidodynamik, Swiss Federal Institute of Technology (ETH),
CH-8092 Zürich, Switzerland

(Received 25 January 1993 and in revised form 21 June 1993)

Experiments are presented for three turbulent boundary layers generated by laterally converging, laterally diverging and parallel flow on a flat plate. A converging potential flow field outside the boundary layer was generated by superposing a parallel flow in the x -direction, a row of equally spaced line sources in the wall-normal (y) direction and an analogous row of sinks in the transversal (z) direction. This arrangement resulted in a velocity that was constant far upstream, far downstream and along the x -axis. The convergence $-\partial W/\partial z$ has its maximum in the plane of the source and sink rows. This flow field was realized with the test section shown in figure 1, based on streamlines intersecting a rectangular cross-section far upstream. The diverging flow was generated by reversing the flow direction through the test section.

The tests were conducted at about 42 m/s leading to a unit Reynolds number of $2.5 \times 10^6/\text{m}$ and to a Reynolds number based on the momentum thickness of 4000 to 4700 at the inlet of the test sections, increasing up to 25000 at the outlet. In all three cases the velocity distribution near the wall agreed very well with the logarithmic law of the wall. The wake contribution in the outer layer was considerably increased by convergence and decreased by divergence. The Reynolds stresses, measured with crossed hot-wire probes, and the wall shear stress, measured with a floating-element balance, were generally increased by divergence and decreased by convergence and the same holds true for the mixing length and the turbulent viscosity.

A finite-difference boundary-layer code using a simple turbulence model was used to predict the experimental results. The comparison showed good agreement for the two-dimensional flow, reasonable agreement for the diverging flow and poor agreement for the converging one. Use of the experimentally determined turbulent viscosity as input into the computation did not systematically improve the agreement but excellent agreement was found if it was combined with anisotropy of the turbulent viscosity. It was much more difficult to predict the converging flow as small errors in the crossflow had a large effect on the flow in the plane of symmetry ($z = 0$).

1. Introduction

Most turbulent boundary layers in engineering applications are subject to the basic strain rate $\partial U/\partial y$, where U is the mean velocity in the x -direction and y is the distance from the wall, and to additional strain rates. As the turbulent flow is highly nonlinear it is not possible to simply superpose the effects of the different strains. However, owing

† Present address: McKinsey & Company, Inc, CH-8703 Erlenbach, Switzerland.

‡ Present address: ABB/Asea Brown Boveri AG, CH-5400 Baden, Switzerland.

to the complexity of the phenomena involved, it seems worthwhile to investigate cases with only one extra strain. Current methods cannot predict most complex flows either (Bradshaw 1988), and basic experiments of this type are therefore still needed.

The present experiment investigates the influence of one extra strain rate, namely $\partial W/\partial z$, where z is the spanwise direction and W is the corresponding mean velocity component. Flow fields of this type were generated on the plane $y = 0$ of the test sections shown in figure 1. Lateral streamline divergence has three obvious effects. First, it introduces an additional term into the continuity equation which corresponds to a thinning of the boundary layer as in the case of an axisymmetric body. Secondly, the curvature of the streamlines induces a velocity component normal to the external streamlines (crossflow). Thirdly, it affects the turbulence structure through vortex stretching in the z -direction. The opposite trends are observed for converging streamlines. Most of the results presented will be for the plane of symmetry ($z = 0$). The cases with converging flow (3Dc), with parallel flow (2D) and with diverging flow (3Dd) had almost identical initial conditions and the same experimental equipment was used. They can therefore be directly compared. For 3Dd the boundary-layer thickness δ , the displacement thickness δ_1 and the momentum thickness δ_2 were all decreased compared to 2D while the wall shear stress τ_w and the Reynolds stresses were increased. For 3Dc the opposite holds true. The law of the wall in the form

$$U^+ = 5.62 \log_{10} y^+ + 5.35 \quad (1.1)$$

was an excellent approximation for all three cases while the wake component was reduced for 3Dd and increased for 3Dc. Mixing length and turbulent viscosity were determined with the measured \overline{uv} and $\partial U/\partial y$, where u and v are the velocity fluctuations in the x - and y -directions respectively.

Experiments comparable to ours were recently presented by Saddoughi & Joubert (1991) for a diverging source-like flow. They also presented an excellent survey of the literature and reviewed the state of the art. The present results confirm and extend their findings. Comparable experiments were also conducted on a cylinder-cone geometry by Smits, Eaton & Bradshaw (1979), in a boundary layer on a flat plate carrying an upstream-facing wedge by Anderson & Eaton (1989) and in the plane between two longitudinal vortices created by a delta wing above a test wall by Pauley, Eaton & Cutler (1989). All cases considered diverging flow. Converging and diverging flows were investigated by Patel & Baek (1987*a, b*) on the plane of symmetry of a body of revolution at an angle of attack. General agreement with the present experiments can be observed but the existence of axial pressure gradients in most experiments makes a direct comparison difficult. Earlier experiments with three-dimensional boundary layers are reviewed by Humphreys & van den Berg (1981).

Degani, Smith & Walker (1992) presented a theory for a turbulent boundary layer near a plane of symmetry. Results are given for self-similar flows at high Reynolds numbers and support the existence of the law of the wall. In the present experiment the pressure gradient $\partial p/\partial z$ changes sign with increasing x and a direct comparison with a self-similar flow is therefore not possible.

A finite-difference boundary-layer code developed by Bettelini (1990) and described by Bettelini & Fanneløp (1993) was used to predict the experimental results. Turbulence was modelled with turbulent viscosity equations suggested by Cebeci & Smith (1968). The two-dimensional flow was predicted very well while the agreement was poorer for 3Dd. For 3Dc the prediction of the momentum thickness beyond the section of maximum flow convergence was very sensitive to changes in parameters. Small errors in the crossflow seem to accumulate near the plane of symmetry which has

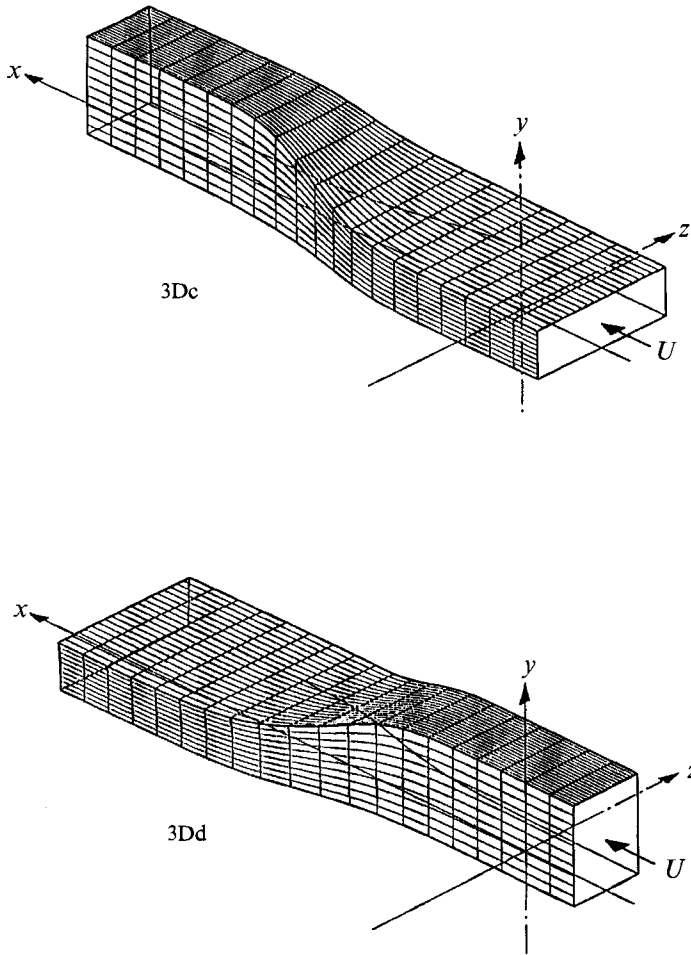


FIGURE 1. Test sections, generating converging (3Dc) and diverging (3Dd) flow above the plane $y = 0$. Velocity U is constant along x -axis.

a considerable influence on the continuity equation and thus on the growth of boundary layer and momentum thickness. Two approaches led to this same problem. In one case, the full problem was solved by following several external streamlines while in the other one, only the flow in the plane of symmetry was considered and the extra term in the continuity equation was taken into account by solving an equation for the spanwise derivative of the crossflow. The problems appeared in both cases. This strong sensitivity is comparable with the case of a laminar boundary layer on a cone at angle of attack, as described by Moore (1956). The diverging flow on the windward side of the cone posed no problems while the converging flow on the leeward side became undetermined before separation of the crossflow took place. An attempt to use the experimentally determined turbulent viscosity as input for the computation met limited success, but excellent agreement was found if it was combined with anisotropy.

In the following section the experimental set-up and the instrumentation will be described. The results will be presented in §3 and in §4 the experiments will be compared with numerical results.

2. Apparatus and measuring techniques

A specially designed boundary layer wind tunnel, shown in figure 2, was used. The test wall ($y = 0$) consisted of a ground stainless-steel plate, 25 mm thick and 4.7 m long carrying a probe holder and the floating-element balance. The steel plate could be moved 2.94 m in the axial direction by a stepper motor with a total accuracy of ± 0.2 mm. This arrangement required a tilting by 3° of the whole tunnel upstream of the test section. The investigated boundary layer was thus formed on the tilted floor of the contraction and deflected by 3° at the junction with the test section. Transition took place more than 2 m upstream of the deflection. A detailed investigation of the boundary layer at $x = 0$ (850 mm downstream of the deflection) showed a standard turbulent boundary layer with excellent two-dimensionality (0.6% r.m.s.-value of the wall shear stress) and a thickness of about 17 mm. The free-stream turbulence was approximately 0.1%. Details of the tunnel geometry and the screens used are given by Pompeo (1992).

The test section was designed for a potential flow with uniform velocity $U_0 = 42$ m/s far upstream, far downstream and along the line $y = 0$, $z = 0$ with a prescribed $\partial W/\partial z(x, 0, 0)$. These conditions can be satisfied by superposing a parallel flow in the x -direction with an infinite row of line sources with strength Q parallel to the y -axis at $x = a$, $z = (2n + 1)d$ with $n = \dots -1, 0, 1, 2, \dots$, and similar line sinks at $x = a$, $y = (2n + 1)d$. With the potential of an infinite row of equidistant line sources given by Lamb (1945) the following velocity field results:

$$\left. \begin{aligned} U(x, y, z) &= U_0 + D(C_{xz} - C_{xy}) \sinh \pi(x-a)/d, \\ V(x, y, z) &= DC_{xy} \sin \pi y/d, \\ W(x, y, z) &= -DC_{xz} \sin \pi z/d, \end{aligned} \right\} \quad (2.1)$$

with

$$C_{xy} = \left[\cosh \frac{\pi(x-a)}{d} + \cos \frac{\pi y}{d} \right]^{-1}, \quad C_{xz} = \left[\cosh \frac{\pi(x-a)}{d} + \cos \frac{\pi z}{d} \right]^{-1}, \quad D = \frac{Q}{4d},$$

Three source-sink elements as described by (2.1) at $a = 625$ mm, 1000 mm, 1375 mm and $d = 1000$ mm were used to design the final test section. The three constants D , one for each source-sink element, were determined with the conditions

$$\begin{aligned} \partial W/\partial z(x = -500 \text{ mm}) &= \partial W/\partial z(x = 2500 \text{ mm}) = -0.015 \text{ s}^{-1}, \\ \partial W/\partial z(x = 1000 \text{ mm}) &= -31.434 \text{ s}^{-1}. \end{aligned}$$

The parameters were chosen to generate a strong convergence on the floor of the test section without risk of flow separation under the roof. The test section was generated by following streamlines that intersected a rectangle (height = 250 mm, width = 800 mm) at $x = -500$ mm to $x = 2500$ mm as shown in figure 1 for (3Dc). The resulting cross-sections deviated slightly from rectangular. As the test section was to be used for flow in either direction, the cross-sections were approximated by rectangles of the same area. The computed pressure field at $y = 0$ and the lateral convergence above the centreline are shown in figures 3 and 7. The test section was built with laminated fibreglass covering styrofoam cores, which resulted in a very stiff configuration with an accuracy better than 0.2° for the direction of the wall normal.

The instrumentation was fairly standard and consisted of: (1) static pressure taps with 0.8 mm diameter; (2) Pitot tubes with Preston-tube geometry and 1 mm and 0.5 mm outer diameter; (3) a three-hole probe manufactured by soldering together three stainless steel tubes with 0.35 mm outer and 0.22 mm inner diameter. The centre tube

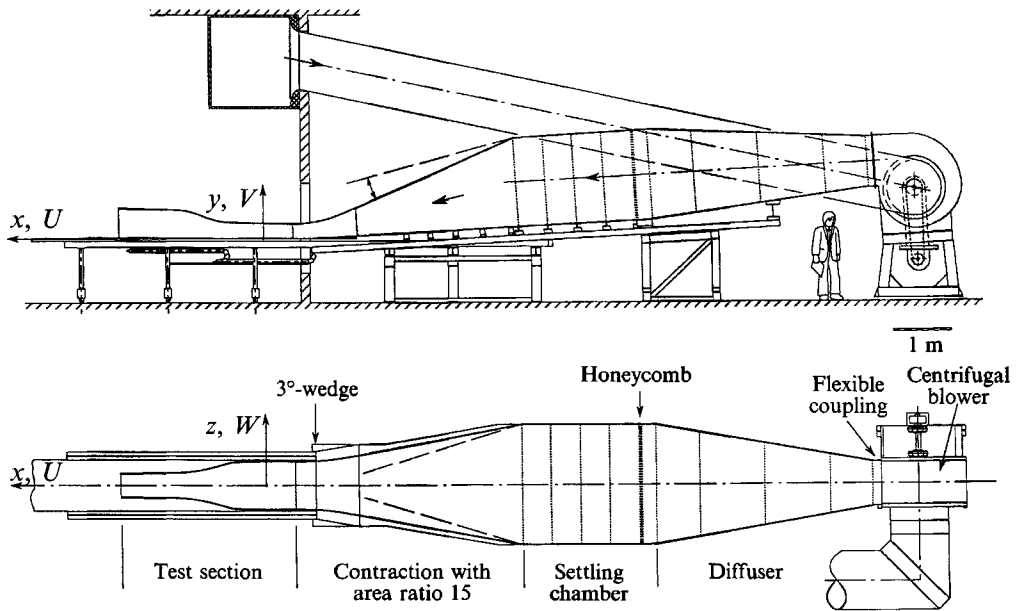
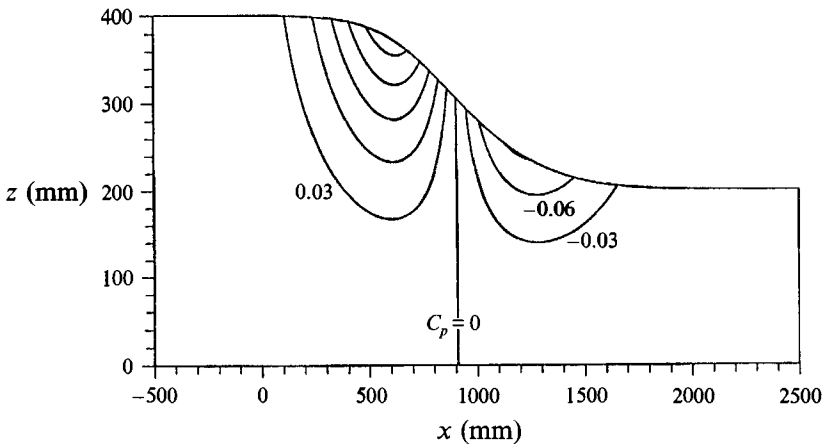


FIGURE 2. The boundary-layer tunnel.

FIGURE 3. Pressure distribution at $y = 0$, $C_p = 2(p - p(0, 0, 0)) / [\rho U(0, 0, 0)^2]$.

was flat ended and the other two had angles of 40° to the probe axes; (4) a five-hole probe with a similar arrangement; (5) crossed hot-wire probes DANTEC 55P61 with 1.25 mm wire length and $5 \mu\text{m}$ wire diameter; (6) a floating-element balance designed by Zurfluh (1984) and described by Hirt, Zurfluh & Thomann (1986). The location of the instruments on the movable test wall is shown in figure 4. The position of the probes was about 100 mm upstream of the probe holder.

All pressures were recorded with a DRUCK PDCR 22 transducer connected to the probes with a Scanivalve scanner. The hot-wire probes were operated with a TSI IFA 100 anemometer with TSI Model 150 bridges, TSI Signal Conditioner Model 157 and TSI IFA 200 A/D-converter. All signals were recorded and reduced by a DEC MicroVAX II. Typical sampling rates were 30000 samples in 3 s for pressure and 10000 samples in 10 s for hot wires.

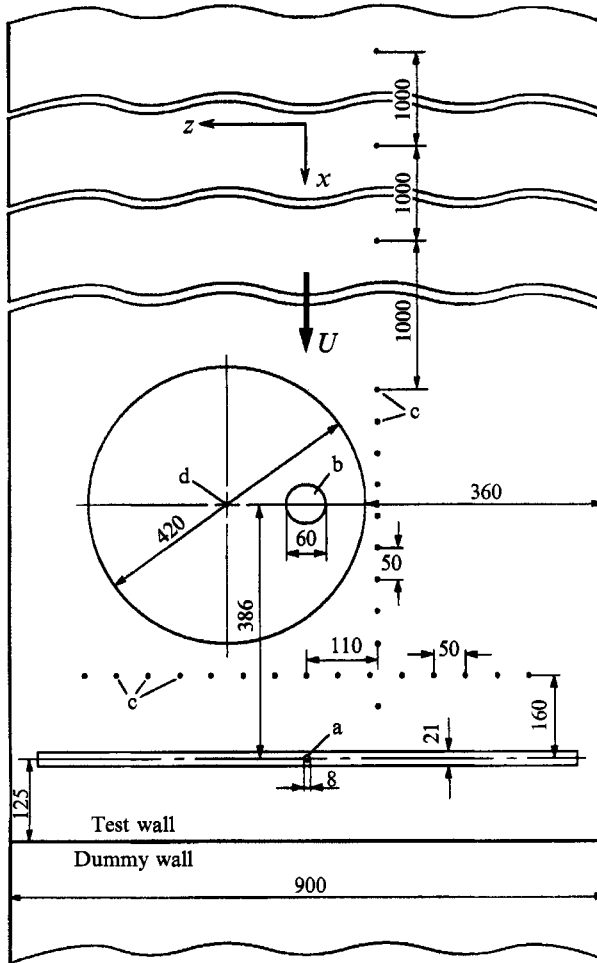


FIGURE 4. Location of probe holder (a), floating element (b), and pressure taps (c). Dimensions in mm.

For the data reduction, the Preston-tube readings Δp_p were reduced to τ_w using the relation suggested by Zurfluh (1984):

$$\frac{\Delta p_p}{\tau_w} = C_1 + C_2(X - X_L) + C_3(X - X_L)^2 + C_4(X - X_L)^3, \quad (2.2)$$

with $X = \log_{10}(\Delta p_p D^2 / 4\rho v^2)$

while for $3.3 < X < 4.8$

$$C_1 = 34.88, \quad C_2 = 32.42, \quad C_3 = 12.44, \quad C_4 = -4.815, \quad X_L = 3.3;$$

for $4.8 < X < 5.7$

$$C_1 = 95.27, \quad C_2 = 37.26, \quad C_3 = -9.220, \quad C_4 = 5.262, \quad X_L = 4.8;$$

and for $5.7 < X < 7.2$

$$C_1 = 125.17, \quad C_2 = 33.45, \quad C_3 = 4.989, \quad C_4 = 0.685, \quad X_L = 5.7.$$

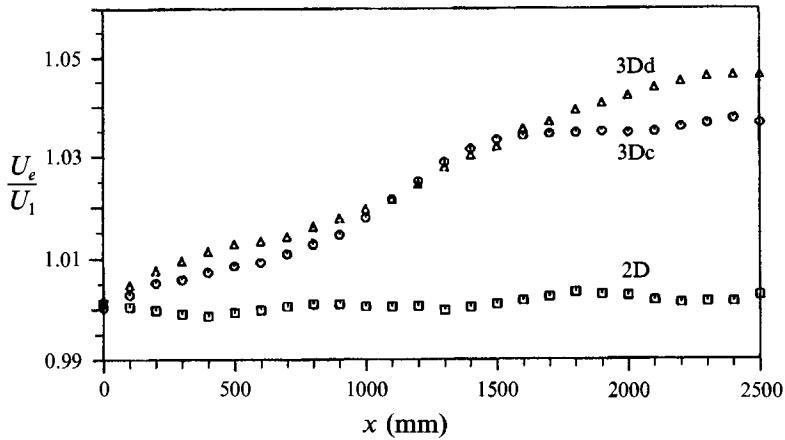


FIGURE 5. Velocity at the outer edge of the boundary layer; $U_1 = U(0, 80 \text{ mm}, 0)$.

The three- and the five-hole probes were always aligned with the x -axis and calibration fields were used to reduce the pressure readings to velocity components.

The Reynolds stress tensor was determined with a crossed hot-wire probe that was rotated into four roll-angle positions. The procedure is described in detail by Anderson & Eaton (1987) and by Pompeo (1992). According to Hirota, Fujita & Yokosawa (1988) the accuracy of this procedure can be improved by using two symmetric probes (long prongs of one probe in place of the short prongs of the second probe). In the present case the symmetry of the test section was used to improve the accuracy in a similar way using only one probe. The geometry of the probe and the probe holder prevented measurements below $y = 3 \text{ mm}$. Three- and four-wire probes were also tested but the accuracy was found to be insufficient (Pompeo & Thomann 1993).

The balance records the torque about its axis d shown in figure 4. The x - and z -components of the wall shear stress could therefore be determined by rotating the balance about point d until the centre of the floating element was at $z = z_0 \neq 0$. Two experiments with the floating element in the same position (x, z_0) but with the balance axis d once upstream and once downstream of the element allowed the determination of the two components of τ_w .

The errors are expected to be below 2% for velocity and τ_w , below 0.3° for angles and below 10% for the Reynolds stresses shown. Details of the equipment, the data reduction and the accuracy can be found in Pompeo (1992).

3. Experimental results

3.1. Mean flow in the plane of symmetry

The velocity U_e at the outer edge of the boundary layer is shown in figure 5. It is practically constant for the 2D test section, which was corrected for the displacement thickness. The 3D test section could not be corrected as it was simply reversed when changing from 3Dc to 3Dd. This resulted in an acceleration of the flow by about 4% for both cases. Figures 6 and 7 show that the measured inviscid flow field agrees well with the predictions based on potential flow in spite of the slight streamwise acceleration.

The wall shear stress $C_f = 2\tau_w/\rho U_1^2$ is shown in figure 8. Balance and Preston tube measurements agree to within 1% or better. The boundary layers at $x = 0$ are slightly

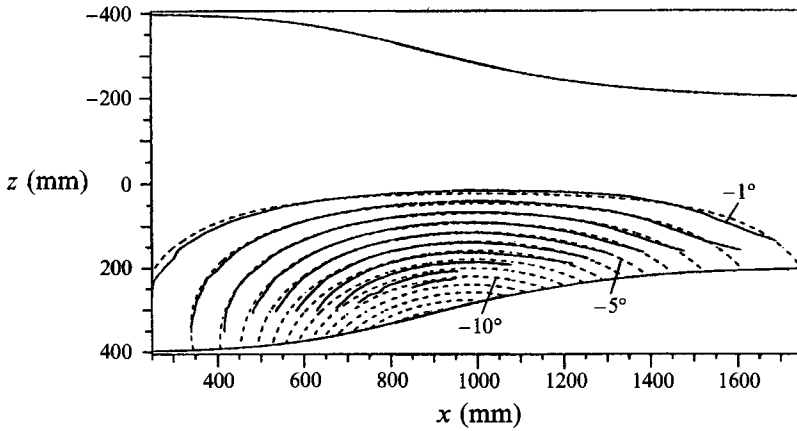


FIGURE 6. Yaw angles at $y = 100$ mm, comparison of experiment (—) with theory (---), 3Dc.

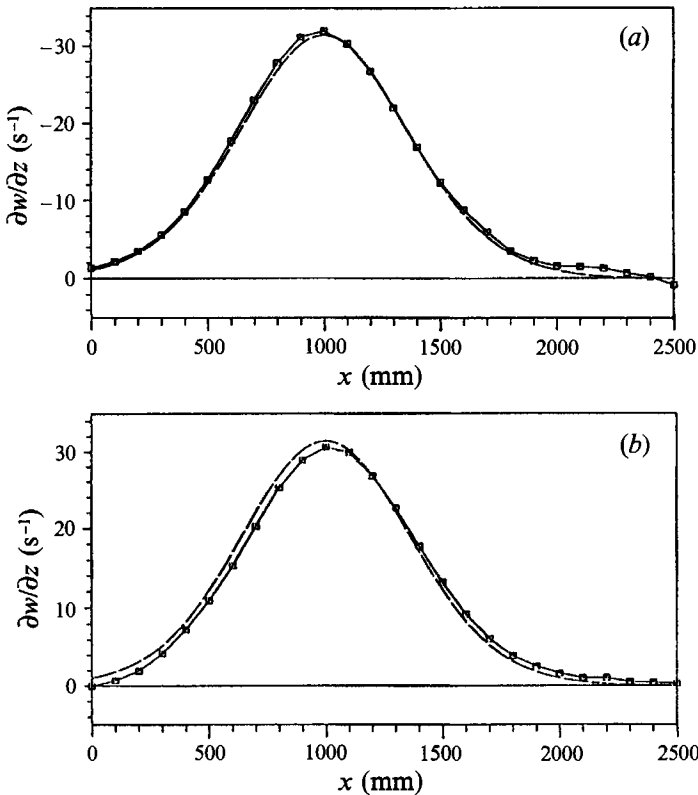


FIGURE 7. (a) Lateral convergence at $y = 100$ mm, $z = 0$. Comparison of experiment (—□—) with equation (2.1) (—); 3Dc, $U_1 = 42$ m/s. (b) Lateral divergence; 3Dd.

different as different inlet sections had to be used. This explains the different results at $x = 0$. The maximum in C_f near $x = 1500$ mm for 3Dd is caused by the decrease of the boundary-layer thickness combined with an increased turbulence intensity.

The velocity profiles were measured with Pitot probes with 1 mm diameter. They are shown in figure 9 and demonstrate the existence of the law of the wall (equation (1.1))

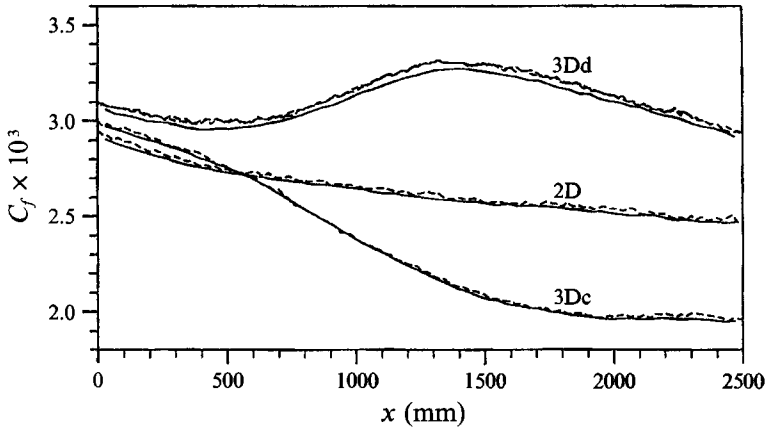


FIGURE 8. Wall shear stress; $C_f = 2\tau_w/\rho U_1^2$; —, balance; - - - - , 1 mm Preston tube; - · - · - , 0.5 mm Preston tube (3Dd only).

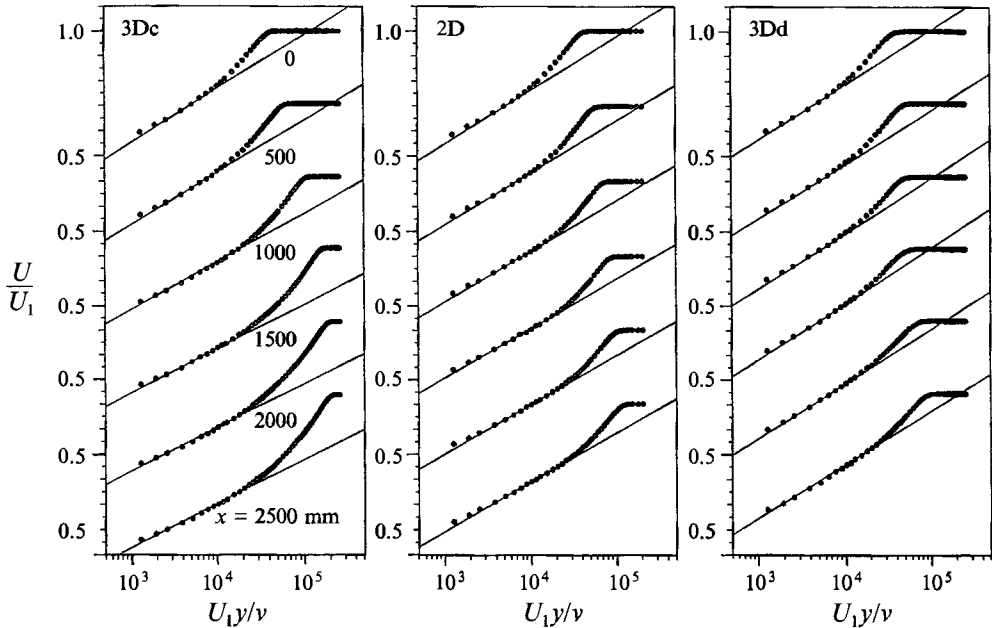


FIGURE 9. Mean velocity profiles; \circ , experiments; —, equation (1.1).

for all three cases. The main difference is in the wake contribution, which is increased by convergence and decreased by divergence.

The boundary-layer thickness $\delta(U(\delta)/U_e = 0.995)$, the displacement thickness δ_1 and the momentum thickness δ_2 are shown in figure 10. As expected, they are increased by convergence and decreased by divergence. The shape parameter $H = \delta_1/\delta_2$ was slightly increased by convergence and decreased by divergence.

3.2. Turbulence in the plane of symmetry

The Reynolds stresses measured in the plane of symmetry of all three test sections are plotted in figures 11 and 12. The level of all turbulence components was decreased by convergence and increased by divergence. The normal stress hierarchy $\overline{u^2} > \overline{w^2} > \overline{v^2}$

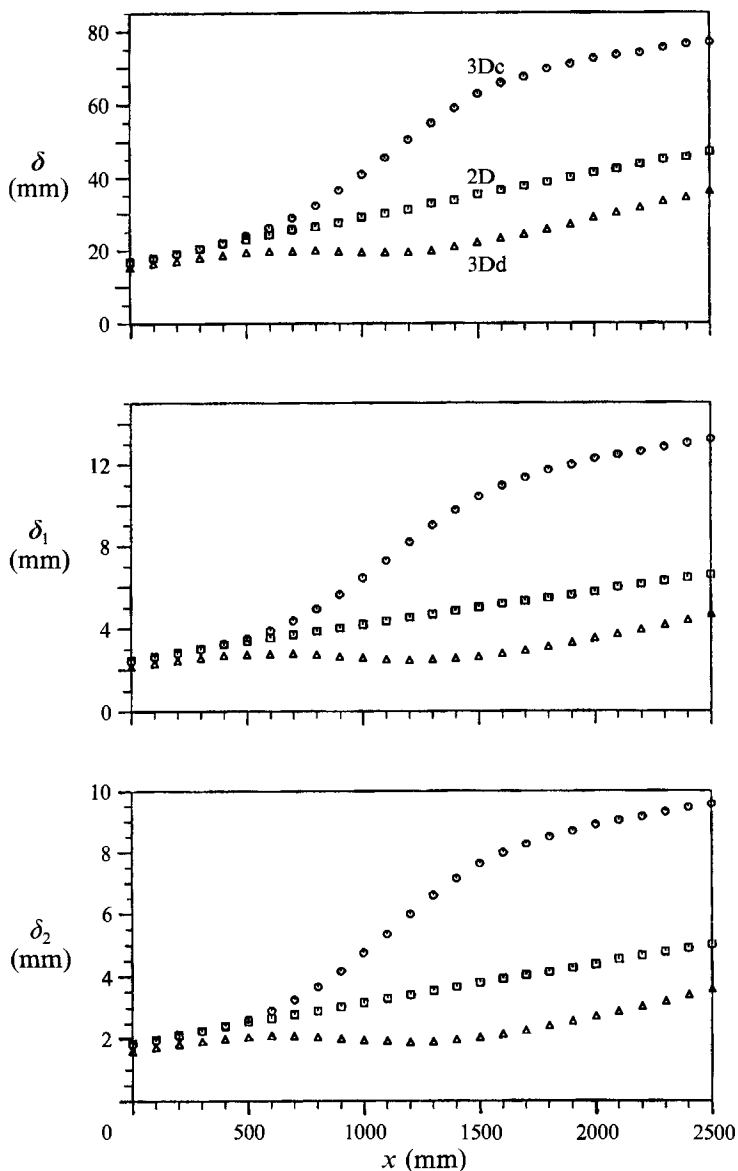


FIGURE 10. Boundary-layer thickness δ , displacement thickness δ_1 and momentum thickness δ_2 in the plane of symmetry.

was maintained in all three cases but changes in the ratios between them can be observed. The measured shear stress extrapolates well to the wall shear stress as measured with the balance.

The turbulent kinematic viscosity ϵ_{11} and the mixing length l are used in many turbulence models. They can be determined with the quantities measured in the present experiments:

$$\epsilon_{11} = \frac{-\overline{uw}}{\partial U / \partial y} \quad (3.1)$$

$$l = \frac{(-\overline{uw})^{1/2}}{\partial U / \partial y}. \quad (3.2)$$

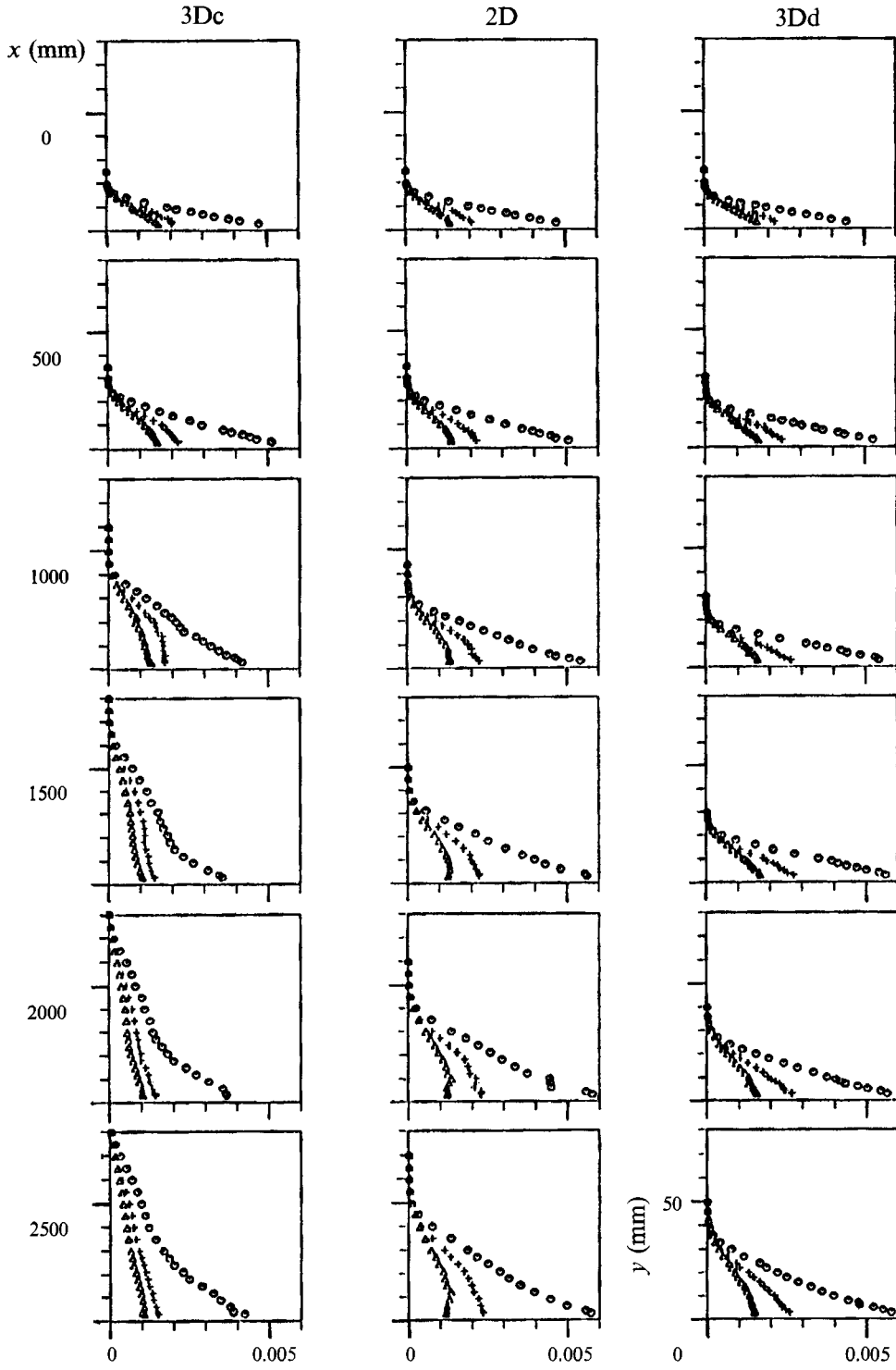


FIGURE 11. Normal stresses measured in the plane of symmetry of the test sections: \diamond , $\overline{u^2}/U_e^2$; \triangle , $\overline{v^2}/U_e^2$; +, $\overline{w^2}/U_e^2$.

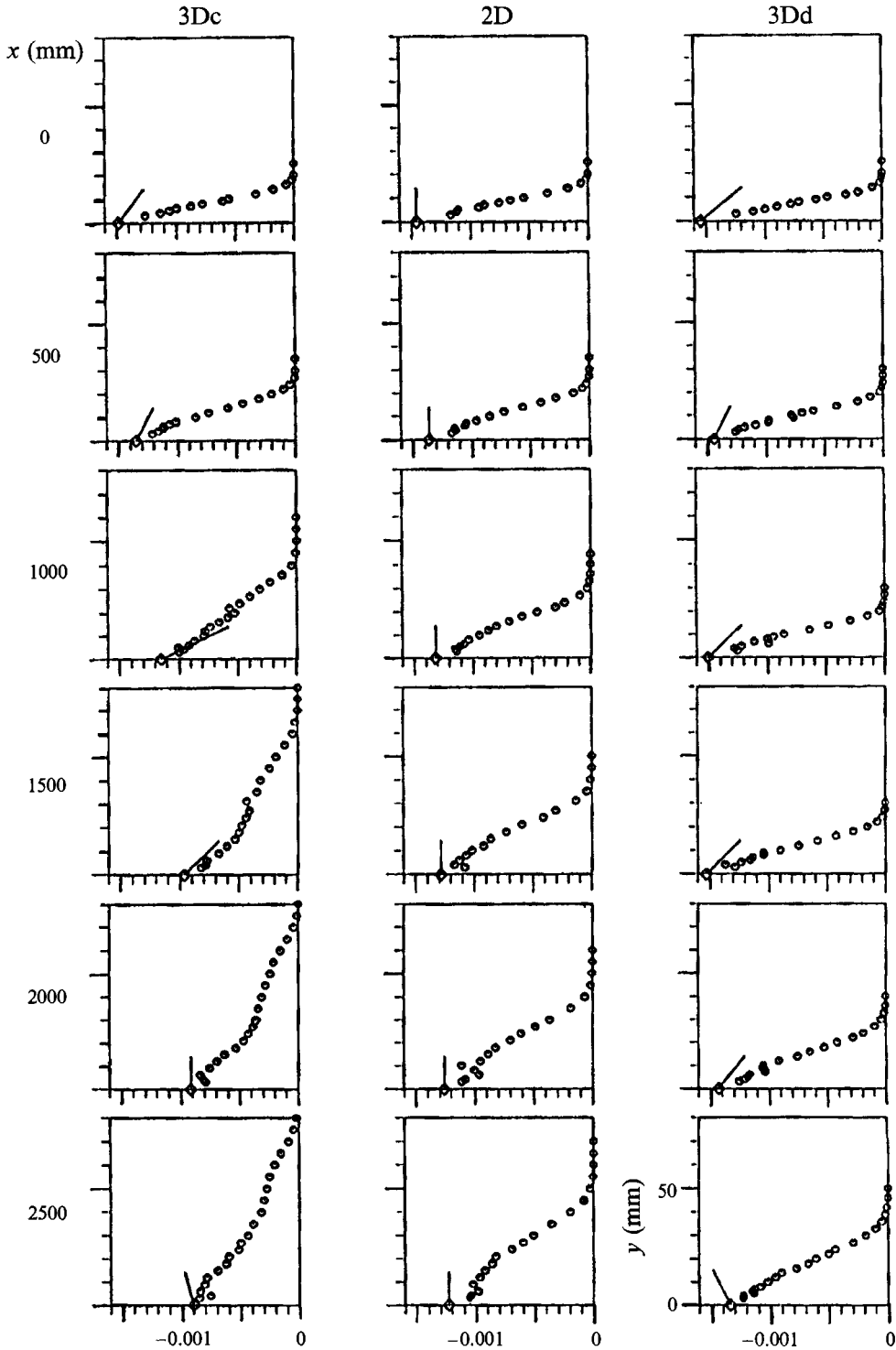


FIGURE 12. Turbulent shear stress measured in the plane of symmetry: \odot , \overline{w} / U_c^2 ; \diamond , wall shear stress measured with the balance; ∇ , $\partial \overline{w} / \partial y$ from $\partial p / \partial x$.

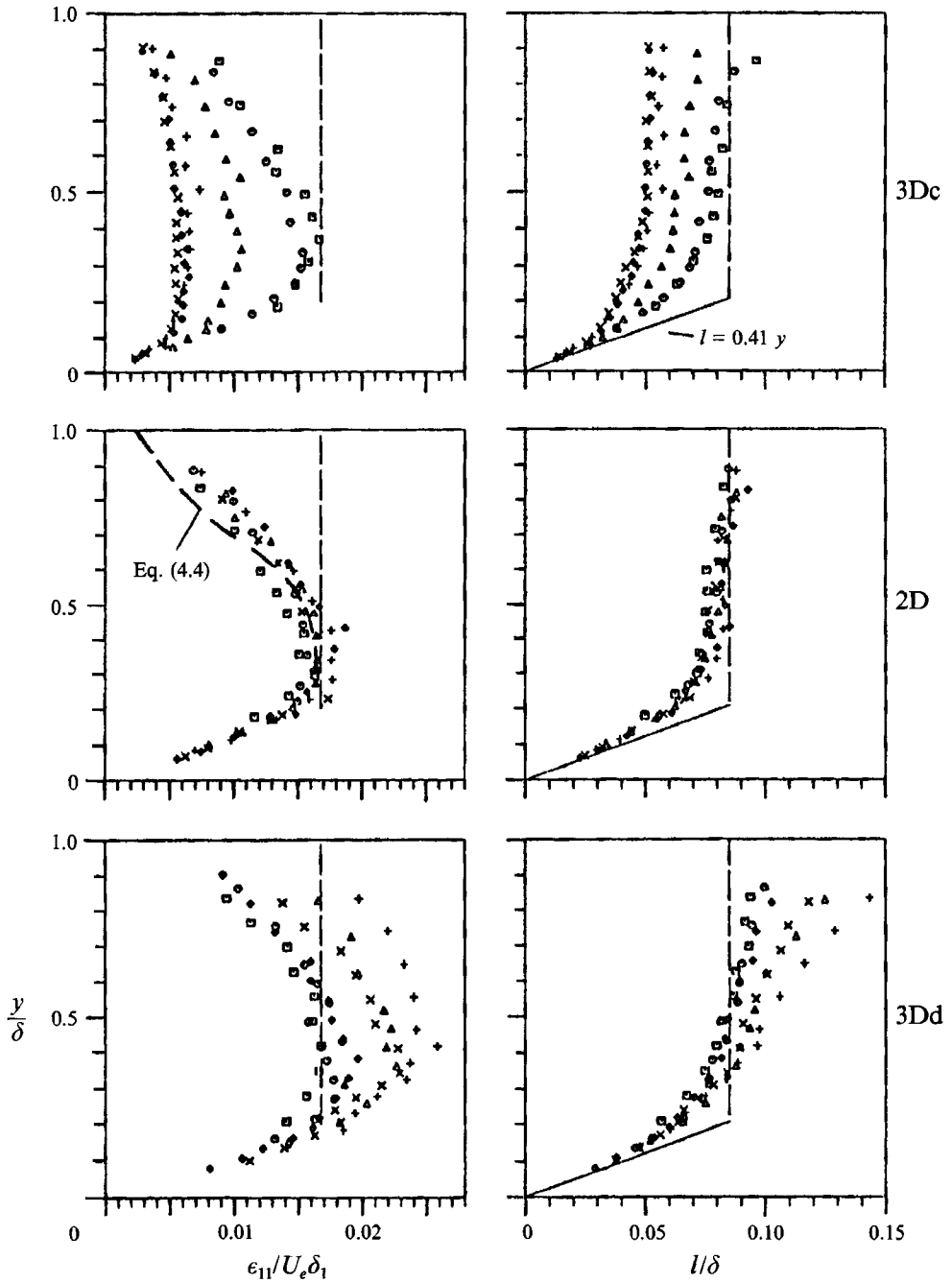


FIGURE 13. Turbulent kinematic viscosity ϵ_{11} and mixing length l measured in the plane of symmetry: \square , $x = 0$ mm; \circ , 500; \triangle , 1000; $+$, 1500; \times , 2000; \diamond , 2500.

Figure 13 shows that the 2D-flow behaves as expected: little change with x , $l \approx 0.41y$ close to the wall and $l \approx 0.085\delta$ in the outer region. The same is observed for the initial stations of both 3Dd and 3Dc. For the convergent flow a strong decrease with x of both ϵ_{11} and l is found. The rate of decrease is largest near $x = 1000$ mm where $|\partial W/\partial z|$ has its maximum and the flow does not recover between $x = 1500$ mm and 2500 mm where

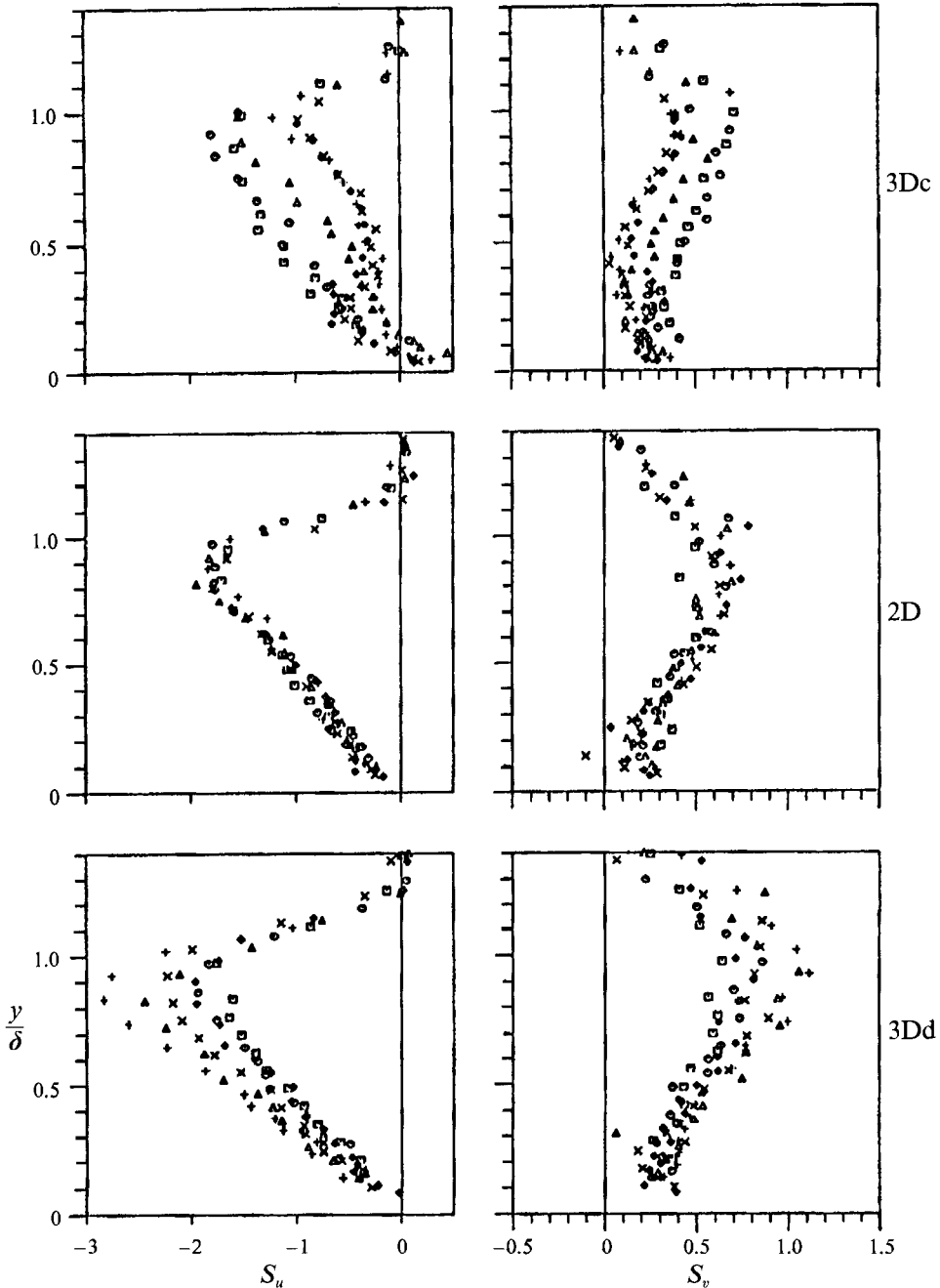


FIGURE 14. Skewness S_u and S_v on the plane of symmetry. Symbols as in figure 13.

$|\partial W/\partial z|$ decreases. The diverging flow shows the opposite behaviour: ϵ_{11} and l increase with x to a maximum near $x = 1500$ mm but recover almost completely between $x = 1500$ mm and 2500 mm. The results for 3Dd are similar to the results reported by Saddoughi & Joubert (1991) who do not show results for converging streamlines.

The following turbulence quantities were determined:

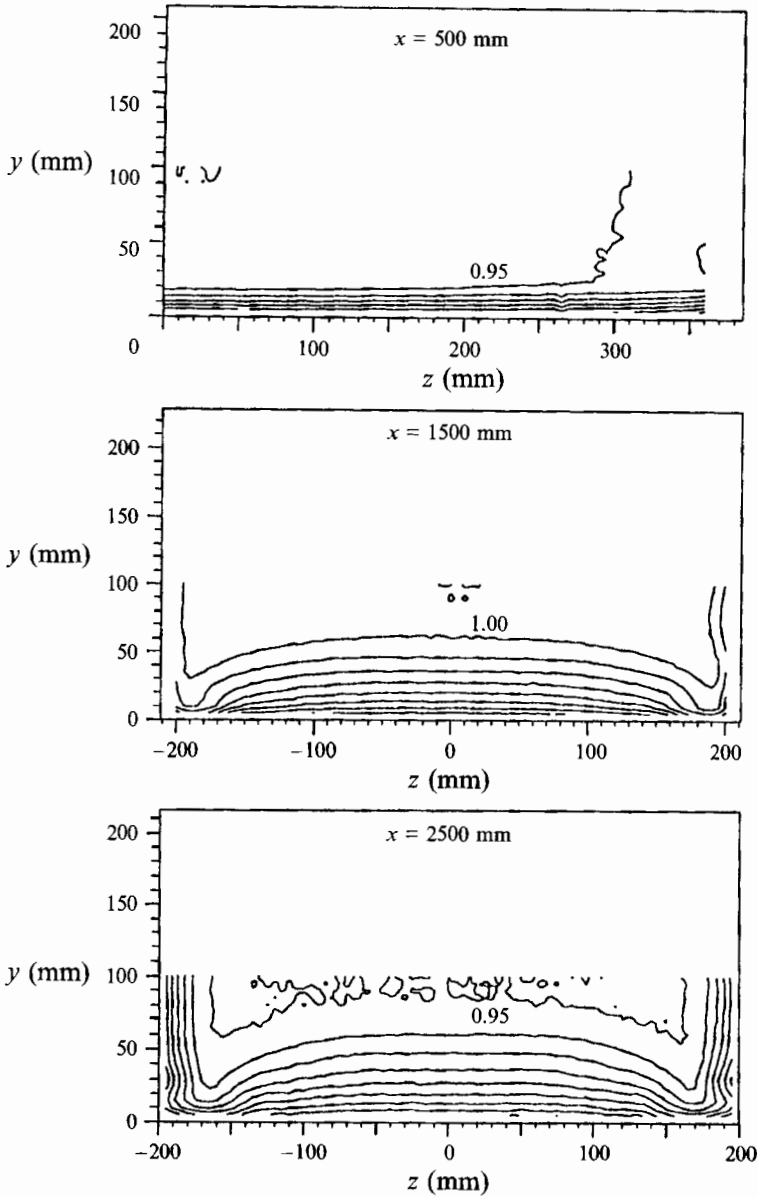


FIGURE 15. Axial velocity distribution U/U_e ($z = 0$); 3Dc; steps between isolines = 0.05.

structural parameter:
$$a_1 = \frac{-\overline{uv}}{\overline{u^2 + v^2 + w^2}}, \quad (3.3)$$

correlation coefficient:
$$R_{uv} = \frac{-\overline{uv}}{(\overline{u^2 v^2})^{1/2}}, \quad (3.4)$$

skewness factors:
$$S_u = \frac{\overline{u^3}}{(\overline{u^2})^{3/2}}, \quad S_v = \frac{\overline{v^3}}{(\overline{v^2})^{3/2}}, \quad (3.5)$$

flatness factors:
$$F_u = \frac{\overline{u^4}}{(\overline{u^2})^2}, \quad F_v = \frac{\overline{v^4}}{(\overline{v^2})^2}. \quad (3.6)$$

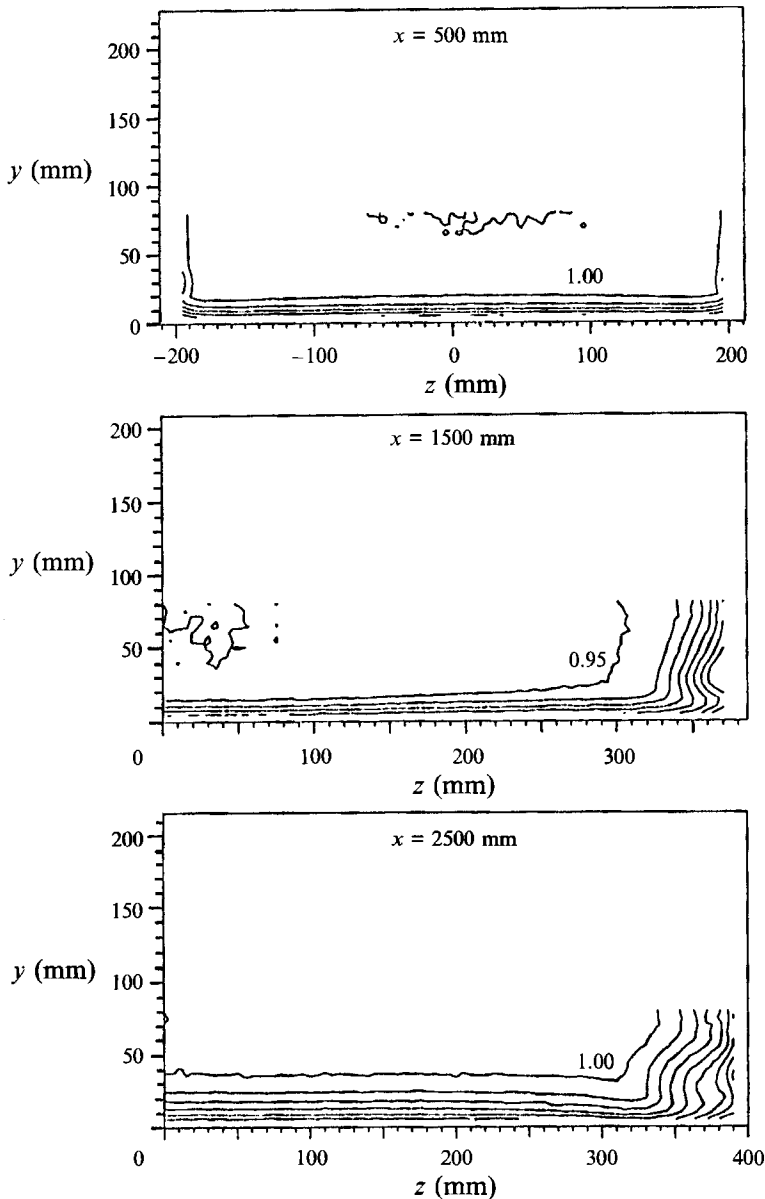


FIGURE 16. Axial velocity distribution $U/U_e(z=0)$; 3Dd; steps between isolines = 0.05.

It is interesting to note that a_1 , R_{uv} , F_u and F_v are essentially independent of convergence and divergence and that a_1 is close to 0.15 as suggested by Bradshaw, Ferris & Atwell (1967). The skewness factors S_u and S_v shown in figure 14, on the other hand, show a significant variation, similar in trend to ϵ_{11} and l in figure 13. As the skewness is an odd function it indicates that the signal is more spiky for 3Dd and less so for 3Dc.

3.3. Flow outside the symmetry plane

The main interest of this paper is directed towards the plane of symmetry. In spite of this, some results of the full flow are presented as additional information. The thickening of the boundary layer by convergence and the thinning by divergence are

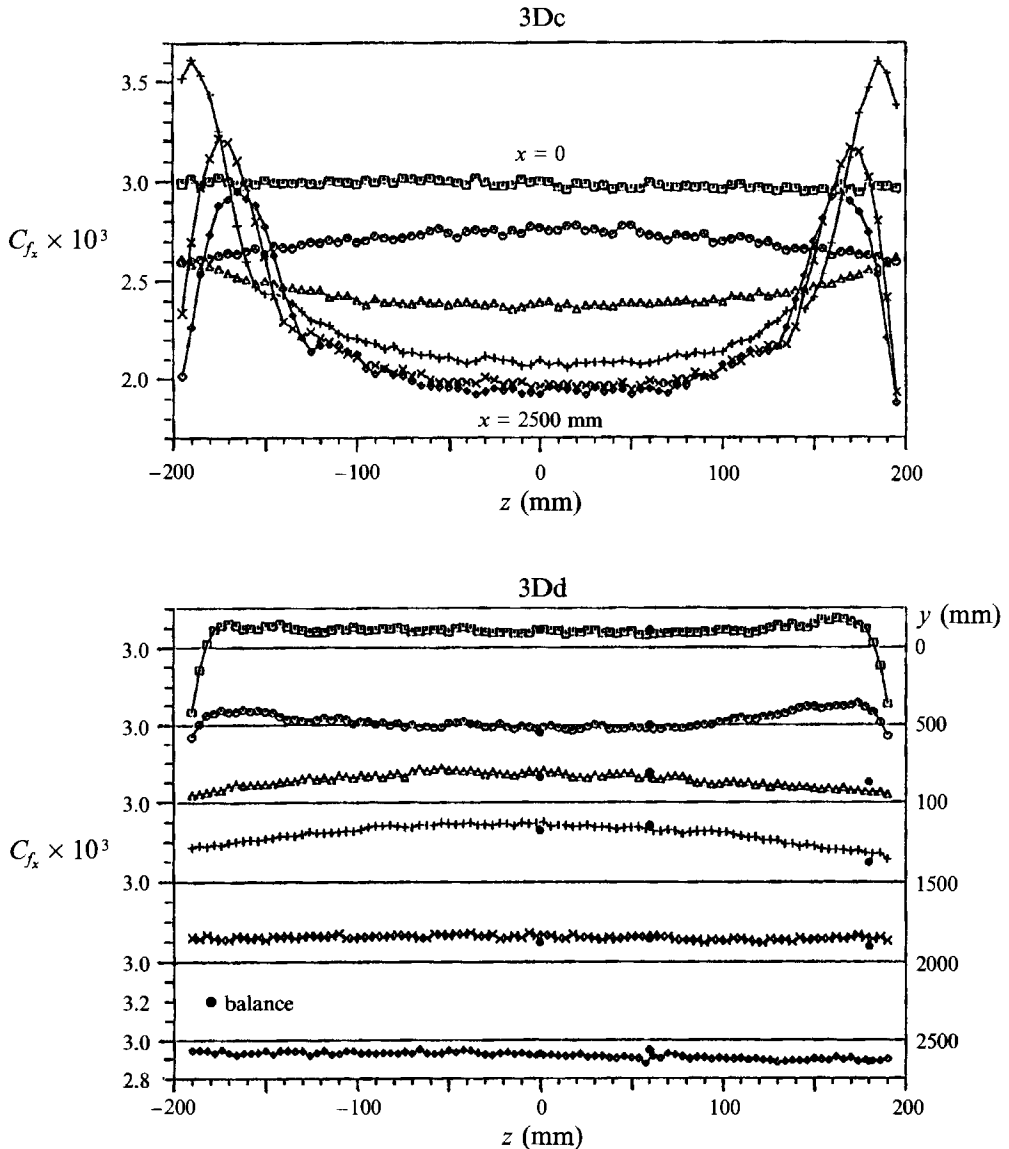


FIGURE 17. Wall shear stress for 3Dc and 3Dd compared with the reading of the balance.

once more illustrated in figures 15 and 16. The axial velocity U was determined with the five-hole probe. The significant change of δ with z for 3Dc and $x \geq 1500$ mm is in strong contrast with the uniform $\delta(z)$ for 3Dd. This is consistent with the $C_{f_x}(x, z)$ shown in figure 17. The C_{f_x} were determined from the readings of a 1 mm Preston tube with its axis parallel to the x -axis. The balance readings at $z = 60$ and 180 mm were determined as described in §2. They are in good agreement with the Preston-tube results.

The crossflow profiles in figure 18 complete the picture of the three-dimensional mean flow field. The change of direction of the profiles between $x = 1000$ and 1500 mm is due to the change of sign of $\partial p / \partial z$ illustrated in figure 3.

The Reynolds stresses shown in figures 11 and 12 were also determined at $x =$

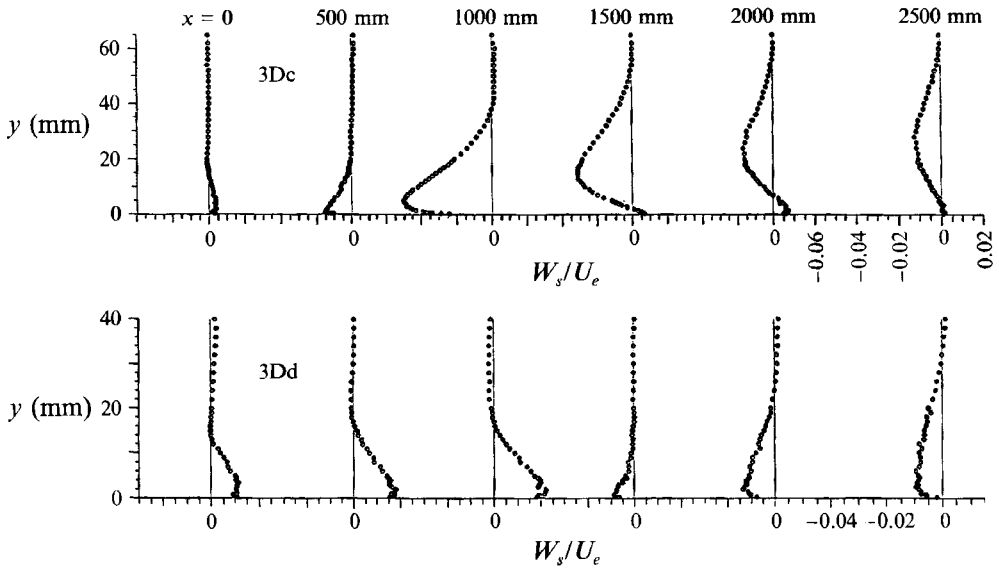


FIGURE 18. Cross-flow profiles W_s/U_e in streamline coordinates at $z = 100$ mm.

(a)		(b)	
Contribution to the continuity equation	Mass flow (kg/s)	Contribution to the momentum equation	Momentum flux or force (N)
$\int_I \rho U dS$	0.8939	$\int_I \rho(U^2 + \bar{u}^2) dS$	$-(36.7269 + 0.0348)$
$\int_O \rho U dS$	-0.8349	$\int_O \rho(U^2 + \bar{u}^2) dS$	$32.3386 + 0.0558$
$\int_R \rho W dS$	0.1040	$\int_R \rho(UW + \bar{u}\bar{w}) dS$	$-3.7357 + O(0)$
$\int_L \rho W dS$	0.1148	$\int_L \rho(UW + \bar{u}\bar{w}) dS$	$-4.1228 + O(0)$
$\int_T \rho V dS$	-0.2884	$\int_T \rho(UV + \bar{u}\bar{v}) dS$	$12.3995 + 0$
Total	-0.0106	$-\int_I p_{st} dS$	-1.4672
		$\int_O p_{st} dS$	0.9116
		$\int_B \tau_{wx} dS$	0.9797
		Total	0.5978

TABLE 1. (a) Integral mass balance and (b) integral momentum balance, 3Dc; I : in at $x = 0$; O : out at $x = 900$ mm; R, L : right and left at $z = \pm 200$ mm; T : top at $y = 50$ mm; B : bottom at $y = 0$.

1000 mm and $z = 100$ and 200 mm for 3Dc and 3Dd. No change of the normal stresses with z could be observed while \overline{w} seemed to decrease by a few percent between $z = 0$ and 200 mm for both test sections.

3.4. Verification of the conservation laws

The time-averaged integral form of the continuity and the momentum equations were applied to a control volume located between $x = 0$ and 900 mm, $y = 0$ and 50 mm and $z = -200$ and +200 mm of 3Dc. The contributions to the two equations are given in table 1(a) and 1(b). They show that the difference between in- and outgoing mass was 0.9% of the ingoing mass while the corresponding figure for the momentum equation is 1.3%.

4. Comparison with computed results

The experiments described in §3 will be compared with results computed with a boundary-layer code developed by Bettelini (1990) and described by Bettelini & Fanneløp (1993). The method solves the first-order boundary-layer equations formulated in terms of streamline coordinates by means of a finite-difference technique. The length $ds_1 = e_1 dx_1$ and the velocity component u_1 point in the streamwise direction, $ds_2 = e_2 dx_2$ and u_2 in the crossflow direction and $ds_3 = e_3 dx_3$ and u_3 in the wall-normal direction with $e_3 = 1$. It is first-order-accurate in the streamwise direction. Implicit finite-differences with second-order accuracy are used in the crossflow and in the wall-normal direction.

The transition to turbulence took place more than 2.8 m upstream of the station $x = 0$. The computation was therefore started at $x = 0$ with the measured U -profiles averaged over z and slightly smoothed. Pertinent information is given in figures 9 and 10 for $x = 0$. The small mismatch in C_f shown in figure 19 for $x \leq 60$ mm had a negligible influence on the results. The choice of the boundary conditions at the outer edge of the boundary layer, on the other hand, had a considerable influence on the results for 3Dc. Three approaches were tested: (a) U_e and W_e from experiments, (b) U_e and W_e from potential flow as given by equation (2.1), (c) the same as (b) but with both U_e and W_e multiplied by $U_e(x)/U_1$, as given in figure 5, to take into account the displacement effect of the boundary layer. All three approaches generated the excessive growth of $\delta_2(x)$ near the plane of symmetry shown in figure 20. The good agreement shown in figures 6 and 7 led to the choice of (c) for the results presented here. The computations used 200 grid points in the wall-normal direction, spaced in a geometric progression, and x_1 steps of 0.33δ . Numerical convergence was verified by varying the step sizes.

The flow near the plane of symmetry can be computed by introducing the unknown $S = \partial u_2 / \partial x_2$ instead of u_2 and replacing the momentum equation in the x_2 -direction by its x_2 -derivative. The resulting system has the advantage that it can be solved along the plane of symmetry without taking into account additional streamlines, which reduces the computational effort by an order of magnitude. The results of this method could hardly be distinguished from boundary-layer calculations based on the full three-dimensional system.

The Reynolds stresses were modelled as

$$-\overline{u'_1 u'_3} = \epsilon_{11} \frac{\partial u_1}{\partial x_3} + \epsilon_{12} \frac{\partial u_2}{\partial x_3}, \quad -\overline{u'_2 u'_3} = \epsilon_{21} \frac{\partial u_1}{\partial x_3} + \epsilon_{22} \frac{\partial u_2}{\partial x_3}. \quad (4.1)$$

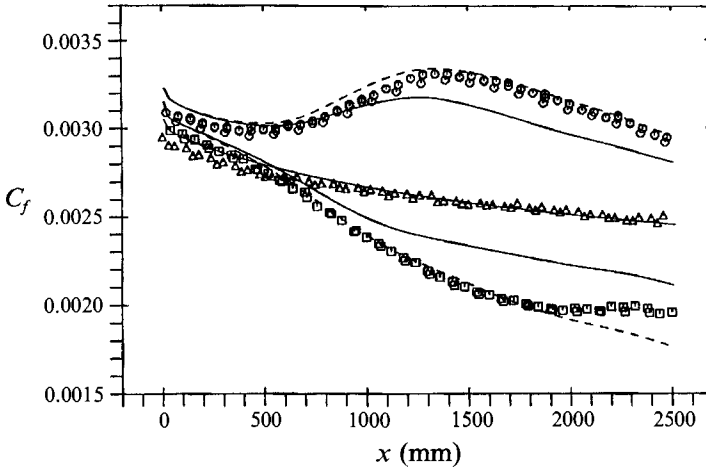


FIGURE 19. Wall shear stress. Experiments: \square , 3Dc; \triangle , 2D; \circ , 3Dd. Predictions: —, step 1; - - -, step 2.

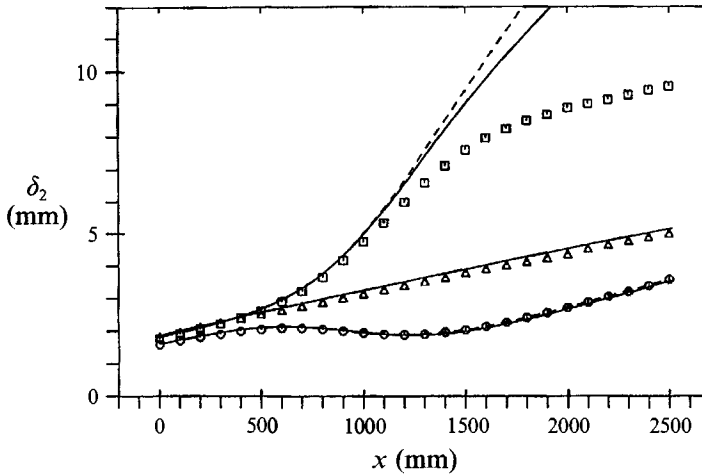


FIGURE 20. Momentum thickness δ_2 , symbols as in figure 19.

In the present case (plane of symmetry) ϵ_{12} does not appear in the equations and $\epsilon_{21} = 0$. An anisotropy parameter E is introduced to connect ϵ_{22} with ϵ_{11} according to

$$\epsilon_{22} = E\epsilon_{11}; \tag{4.2}$$

ϵ_{11} was determined as suggested by Cebeci & Smith (1968).

For $x_3 < x_3^*$:

$$\epsilon_{11} = l^2 \frac{\partial u_1}{\partial x_3}, \tag{4.3}$$

where

$$l = 0.41x_3 D, \quad D = 1 - \exp(-u_\tau x_3 / 26\nu);$$

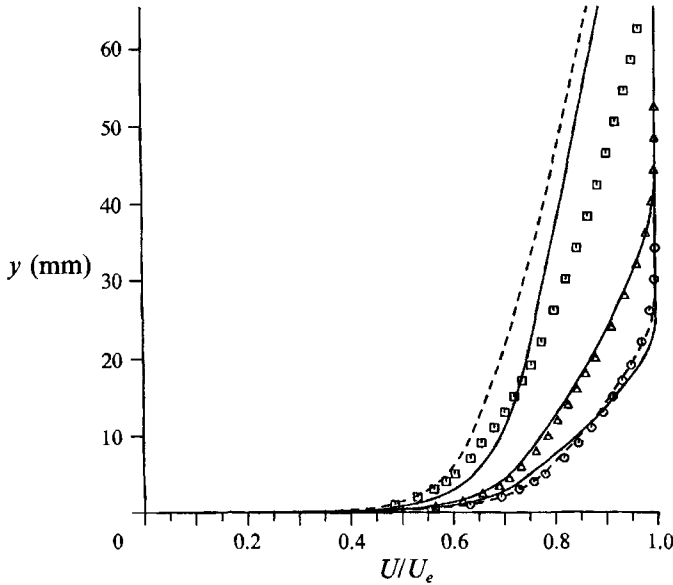
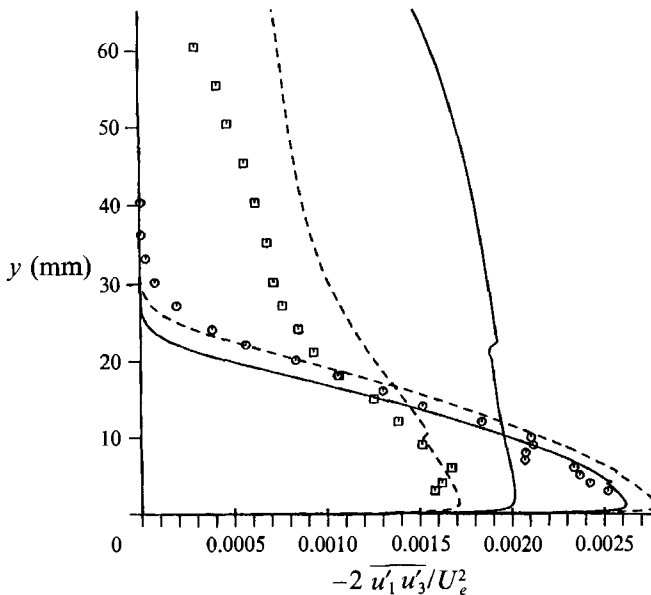
and for $x_3 \geq x_3^*$

$$\epsilon_{11} = KU_e \delta_1 \gamma, \tag{4.4}$$

where

$$K = 0.0168, \quad \gamma = [1 + 5.5(x_3/\delta)^6]^{-1},$$

where x_3^* denotes the smallest wall distance x_3 for which (4.3) and (4.4) assume the

FIGURE 21. Velocity profiles at $x = 2000$ mm, symbols as in figure 19.FIGURE 22. Turbulent shear stress at $x = 2000$ mm, symbols as in figure 19.

same value. U_e , δ , u_τ and ν denote the external velocity, the boundary-layer thickness ($U = 0.999U_e$), the friction velocity and the kinematic viscosity respectively.

The agreement between experiments and computations was improved in several steps which are closer to 'numerical experiments' than to physical reasoning.

Step 1: Standard method

The turbulence model in (4.1)–(4.4) was used. Wall shear stress C_f , δ_2 , typical velocity profiles and shear-stress distributions are shown in figures 19–22. As expected, case 2D was well predicted. In 3Dd the velocity profile, δ_2 and the shear-stress profile

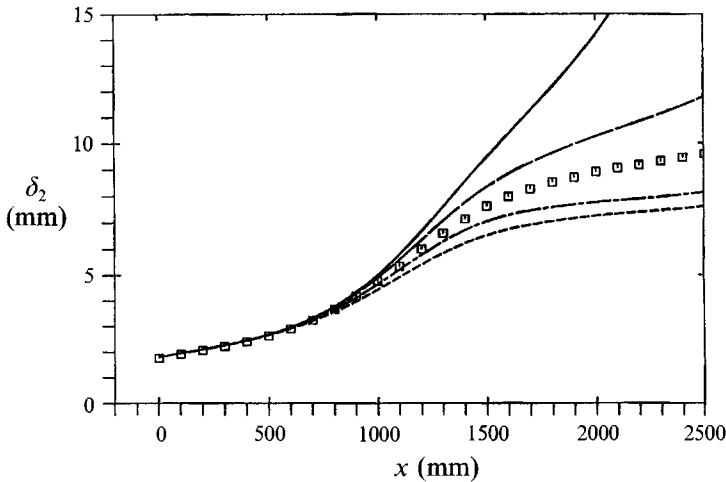


FIGURE 23. Momentum thickness δ_2 , 3Dc. —, $E = 1$; ----, $E = 2$; - · - · -, $E = 10$; · · · · ·, $E = 100$, \square , experiments.

x (mm)	K (3Dc)	K (3Dd)
0	0.0168	0.0168
500	0.0155	0.0175
1000	0.0110	0.0230
1500	0.0060	0.0250
2000	0.0060	0.0230
2500	0.0060	0.0190

TABLE 2. Adjusted constant K in equation (4.4)

were in good agreement while C_f was too low. Case 3Dc was much worse, with δ_2 and shear-stress profiles much too big. In particular, δ_2 was difficult to predict as the sensitivity to step size and initial conditions was much higher than for the other quantities.

Step 2: Adjustment of ϵ_{11} for 3Dc and 3Dd

In an attempt to improve the predictions the turbulence model was adapted to the experimental results. The excellent agreement with the 'law of the wall' shown in figure 9 suggests that (4.3) should not be changed. Experience with the 2D flow indicated that taking into account the measured decrease of ϵ_{11} in 3Dc (figure 13) would reduce the excessive growth of $\delta_2(x)$ observed in figure 20. Equation (4.4) was therefore modified by adapting K as indicated in table 2.

The results (dotted lines in figures 19–21) show good agreement for C_f , but some velocity and shear-stress profiles improved, some deteriorated and the problem with $\delta_2(x)$ remained.

Step 3: Adjustment of ϵ_{22}

An attempt to improve the agreement for 3Dc was based on the following ideas. The mass balance mentioned in §3.4 shows that the outflow through the top of the volume at $y = 50$ mm (0.3 kg/s) is due to the difference between 'in' and 'out' in the flow direction (0.1 kg/s) and to the inflow from the two sides at $z = \pm 200$ mm (twice

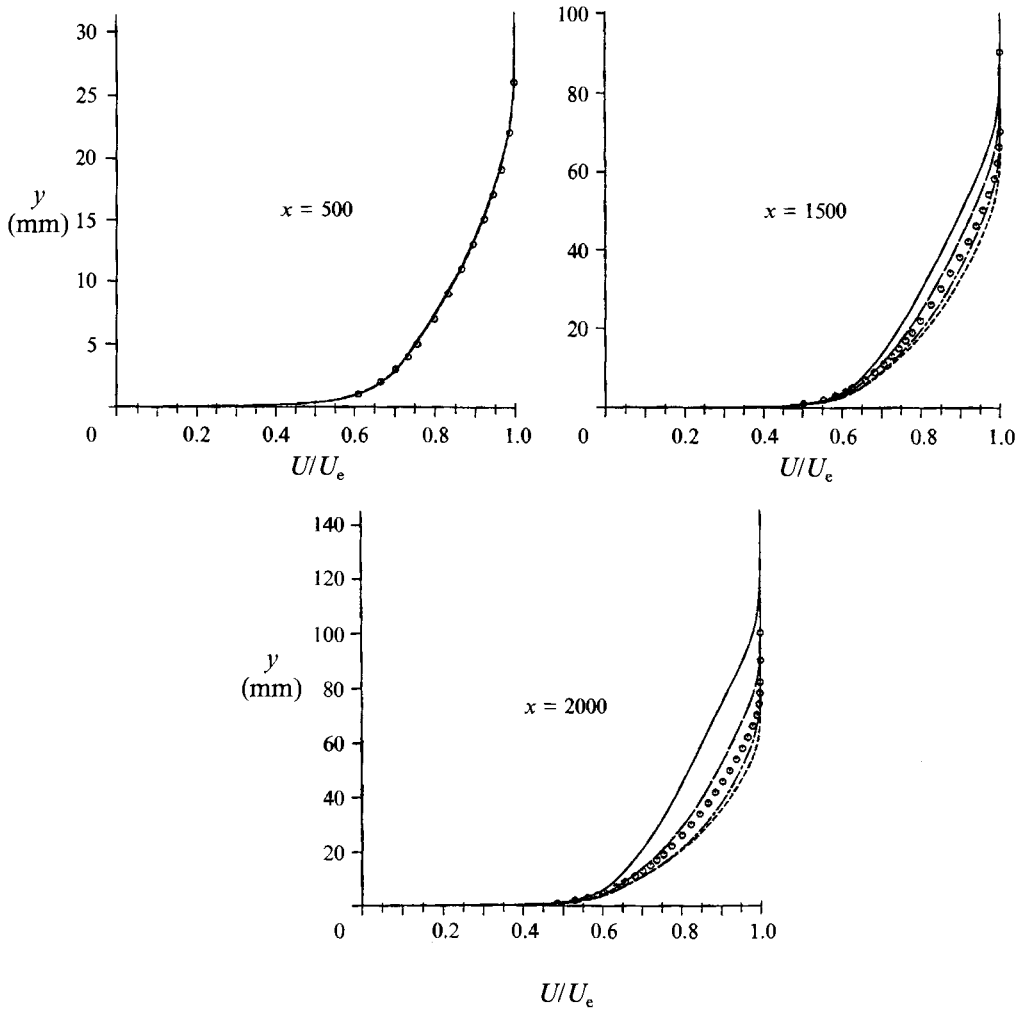


FIGURE 24. Velocity profiles, symbols as in figure 23.

0.1 kg/s). The crossflow therefore contributes considerably to the thickening of the boundary layer. If it is slightly too big, the error will accumulate downstream and result in an excessive growth of boundary layer and momentum thickness. Furthermore, predictions with STAN5 (Crawford & Kays 1976), using the version for a body of revolution without crossflow, resulted in a $\delta_2(x)$ below the experimental values. This suggested that a decrease of the crossflow by increasing $\epsilon_{22} = E\epsilon_{11}$ would decrease the excessive growth of $\delta_2(x)$ and generate more realistic predictions. Big increases of E could be chosen as $E \rightarrow \infty$ would eliminate the crossflow completely, leading to conditions similar to the body-of-revolution flow mentioned above.

The results, shown in figures 23–25 for 3Dc, support this procedure. The best agreement is near $E = 3$ while the computation failed completely for $E < 0.8$ because of excessive growth of δ_2 . Attempts to increase E while keeping $K = 0.0168$ in the expression for ϵ_{11} , or to decrease ϵ_{11} while keeping ϵ_{22} unchanged, were considerably less successful.

Case 3Dd was well predicted with step 2 (figures 19–22) and it proved to be much less sensitive to changes of E . A decrease from $E = 1$ to $E = 0$ could hardly be observed

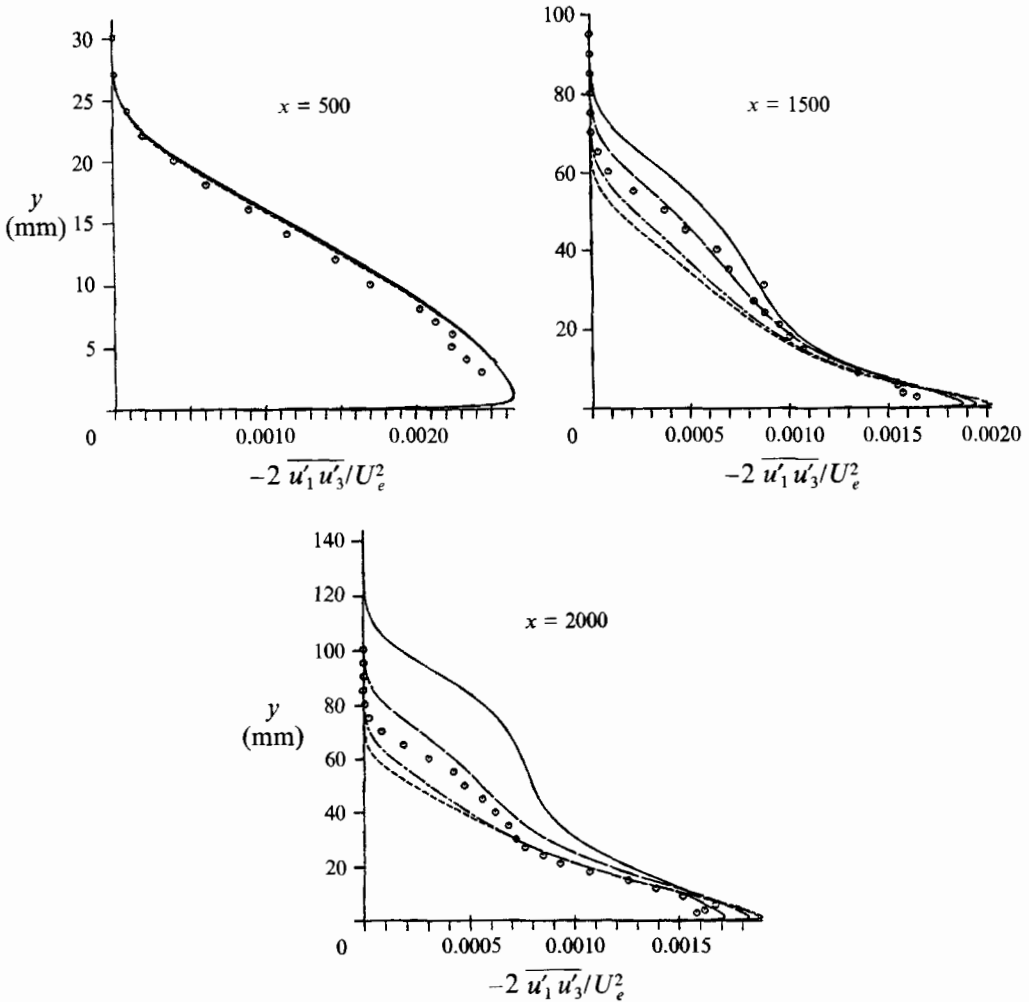


FIGURE 25. Turbulent shear stress, symbols as in figure 23, $\overline{u'_1 u'_3} = \overline{uw}$.

in figures 19–22. This is probably because the crossflow profiles changed their shape considerably while their displacement thickness remained nearly constant. The different sensitivities of converging and diverging flows are also found in the stability analysis by Scholtysik, Bettelini & Fanneløp (1993).

As mentioned before, steps 2 and 3 should be considered as ‘numerical experiments’ guided by physical intuition. The success of step 3 clearly shows the great influence of the crossflow in a converging flow. However, $E \approx 3$ was an unexpected result. The code was therefore carefully checked in the following way:

- (i) independence of step size was verified.
- (ii) 2D laminar boundary layers were very accurately predicted.
- (iii) The self-similar boundary layer formed on a plane wall at $x_3 = 0$ under a fluid in solid-body rotation about the x_3 -axis (Schlichting 1982), was very well predicted.
- (iv) The results for the 2D turbulent boundary layer agreed well with the experiments, figures 19–21.
- (v) The fully 3D boundary-layer calculations agreed very well with the calculations restricted to the plane of symmetry.

(vi) Decreasing the crossflow by arbitrarily increasing the crossflow viscosity led to results that agreed well with results for a corresponding body of revolution (no crossflow) simulated with STAN5.

5. Conclusions

Experimental results for turbulent boundary layers near a plane of symmetry are presented. The boundary layers were subject to lateral convergence and divergence while the acceleration in the flow direction was kept negligible.

In the outer part of the boundary layer the skewness and the turbulent viscosity were considerably reduced by convergence and increased by divergence while excellent agreement with the 'law of the wall' was found close to the wall.

The prediction of the diverging flow agreed well with the measurement and posed no special problems. The prediction of the converging flow, on the other hand, was very difficult. Small errors in the crossflow accumulate near the plane of symmetry and have a considerable influence on the continuity equation and thus on boundary layer and momentum thickness which leads to bad agreement. Little improvement was obtained by taking into account the measured decrease of the turbulent viscosity. Combining this decrease with a simple anisotropy to adjust the strength of the crossflow resulted in excellent agreement, demonstrating the importance of the crossflow. The authors do not believe that these 'fixes' (decrease of K and increase of E) are universal and can be used in other computations. They serve, however, as warning that simple turbulence models might fail. The prediction of this converging flow should therefore be a very good test for computational methods.

All data presented here and by Pompeo (1992) are available on 3.5" floppy discs from the third author.

REFERENCES

- ANDERSON, S. D. & EATON, J. K. 1987 An experimental investigation of pressure-driven three-dimensional turbulent boundary layers. *Stanford University, Thermosci. Div. Rep.* MD-49.
- ANDERSON, S. D. & EATON, J. K. 1989 Reynolds stress development in pressure-driven three-dimensional turbulent boundary layers. *J. Fluid Mech.* **202**, 263–294.
- BRADSHAW, P. 1988 Effects of extra rates of strain – review. *Zoran Zaric Memorial Sem., Dubrovnik. Hemisphere.*
- BRADSHAW, P., FERRIS, D. H. & ATWELL, N. P. 1967 Calculation of boundary-layer development using the turbulent energy equation. *J. Fluid Mech.* **28**, 593–616.
- BETTELINI, M. S. G. 1990 Numerical study of some engineering turbulence models for three-dimensional boundary layers. Dissertation, ETH No. 9182.
- BETTELINI, M. S. G. & FANNELØP, T. K. 1993 A systematic comparison of mathematically simple turbulence models for three-dimensional boundary layers. *AIAA J.* **31**, 999–1006.
- CEBECI, T. & SMITH, A. M. O. 1968 A finite-difference solution of the incompressible turbulent boundary-layer equations by an eddy-viscosity model. In *1968 AFOSR-IFP-Stanford Conf. on Computation of Turbulent Boundary Layers* (ed. S. J. Klein *et al.*). Stanford University.
- CRAWFORD, M. E. & KAYS, W. M. 1976 STAN5 – A program for numerical computation of two-dimensional internal and external boundary layer flows. *NASA CR* 2742.
- DEGANI, A. T., SMITH, F. T. & WALKER, J. D. A. 1992 The three-dimensional turbulent boundary layer near a plane of symmetry. *J. Fluid Mech.* **234**, 329–360.
- HIROTA, M., FUJITA, H. & YOKOSAWA, H. 1988 Influences of velocity gradient on hot-wire anemometry with an X-wire probe. *J. Phys. E: Sci. Instrum.* **21**, 1077–1084.
- HIRT, F., ZURFLUH, U. & THOMANN, H. 1986 Skin friction balances for large pressure gradients. *Exps Fluids* **4**, 296–300.

- HUMPHREYS, D. A., VAN DEN BERG, B. 1981 Three-dimensional turbulent boundary layers. In *1980-81 AFOSR-HTTM-Stanford Conf. on Turbulent Flows* (ed. S. J. Kline, B. J. Cantwell & G. M. Lilley). Stanford University.
- KLINE, S. J., CANTWELL, B. J., LILLEY, G. M. (Ed.) 1981 Complex turbulent flows. *1980-81 AFOSR-HTTM-Stanford Conference on Turbulent Flows*. Stanford University.
- KLINE, S. J., MORKOVIN, M. V., SOVRAN, G., COCKRELL, D. J., COLES, D. E., HIRST, E. A. (Ed) 1968 *Proc. Computation of Turbulent Boundary Layers*. 1968 AFOSR-IFP-Stanford Conference, Stanford University.
- LAMB, H. 1945 *Hydrodynamics*, 6th edn. Dover.
- MOORE, F. K. 1956 Three-dimensional boundary layer theory. *Adv. Appl. Mech.* **IV**, 159-228.
- PATEL, V. C. & BAEK, J. H. 1987*a* Boundary layers in planes of symmetry. Part I: Experiments in turbulent flow. *AIAA J.* **25**, 550-559.
- PATEL, V. C. & BAEK, J. H. 1987*b* Boundary layers in planes of symmetry. Part II: Calculations for laminar and turbulent flows. *AIAA J.* **25**, 812-814.
- PAULEY, W., EATON, J. & CUTLER, A. 1989 Diverging boundary layers with zero streamwise pressure gradient. *AIAA Paper* 89-0134.
- POMPEO, L. 1992 An experimental study of three-dimensional turbulent boundary layers. Dissertation, ETH No 9780.
- POMPEO, L. & THOMANN, H. 1993 Quadruple hot-wire probes in a simulated wall flow. *Exps Fluids* **14**, 145-152.
- SADDOUGHI, S. G. & JOUBERT, P. N. 1991 Lateral straining of turbulent boundary layers. Part 1. Streamline divergence. *J. Fluid Mech.* **229**, 173-204.
- SCHLICHTING, H. 1982 *Grenzschicht-Theorie*. G. Braun.
- SCHOLTYSIK, M., BETTELINI, M. S. G. & FANNELØP, T. K. 1993 A note on problems in 3D boundary layer computations in streamline coordinates. *Z. Angew. Math. Phys.* (to appear).
- SMITS, A. J., EATON, J. A. & BRADSHAW, P. 1979 The response of a turbulent boundary layer to lateral divergence. *J. Fluid Mech.* **94**, 243-268.
- ZURFLUH, U. E. 1984 Experimentelle Bestimmung der Wandschubspannung in turbulenten Grenzschichten. Dissertation, ETH No 7528.